Geophys. J. R. astr. Soc. (1967) **13**, 149–159.

The Krakatoa Air–Sea Waves: an Example of Pulse Propagation in Coupled Systems

David Harkrider and Frank Press

Summary

The theory of pulse propagation in an atmosphere coupled to an ocean is applied to the air–sea waves excited by the explosion of the volcano Krakatoa. Numerical results for a realistic atmosphere–ocean system show that the principal air pulse corresponds to the fundamental gravity mode GR_0. A small sea wave is associated with the mode GW_0 with phase velocities close to the $\sqrt{(gh)}$ velocity of the ocean. Free waves with this velocity exist in the atmosphere and transfer energy to the ocean in an efficient manner. These air waves 'jump' over land barriers and re-excite the sea waves. An explosion of 100–150 megatons is required to produce the equivalent of the Krakatoa pressure disturbance.

1. Introduction

In recent years theoretical–numerical techniques have become available which make possible the computation of dispersion curves, excitation functions, and synthetic time series for elastic–gravity wave propagation in realistic systems (see, for example, Press & Harkrider 1962, Harkrider 1964). It is a simple matter to extend these techniques to a coupled system like that formed by the atmosphere and ocean.

In this paper we apply these methods in an attempt to explain the sea waves which were observed at large distances from the explosion of the volcano Krakatoa in 1883. The early arrival of these waves at most stations eliminated the possibility that they were gravity waves on the ocean following all-water paths. Since the arrival time of the major tide-gauge disturbances could be correlated with the arrival time of the first or second air waves, Ewing & Press (1955) suggested that the energy in the sea wave was transferred to the water from the air wave by resonant coupling when this disturbance approached the station from the ocean side, but they were unable to identify a free wave in the ocean which matched the phase velocity of 312 m/s of the atmospheric pulse.

The theory of the subject was left unexplained, since no tools were then available to compute dispersion and amplitudes for the atmosphere–ocean coupled system with a specified source and receiver.

The essence of our explanation is that the atmosphere alone supports many modes of internal waves with phase velocities and group velocities in the range of long mid-ocean gravity waves. The sea waves will be excited by a transfer of energy from the atmosphere to the ocean, the amount depending on the length of path over the ocean leading to the station.

2. Theoretical–numerical methods

In the atmospheric pulse propagation theory (Press & Harkrider 1962, Harkrider 1964) a standard temperature model of the Earth's atmosphere is approximated by

isothermal layers terminated at 220 km by either an isothermal half-space, a free surface, or a rigid surface. As long as the layer thickness is small compared to its distance from the Earth's centre, the radial dependence of excess pressure can be approximated by the vertical z dependence for a plane isothermal layered gravitating medium. The resulting solution for a source and receiver in the plane layered problem is approximately corrected for sphericity by using the colatitude dependence which near the source approaches the flat-Earth horizontal r dependence.

The source used to model the Krakatoa eruption in this paper is the azimuthally symmetric Green's function for an isothermal gravitating space (Harkrider 1964). With this source at an altitude H, the excess pressure at the Earth's rigid surface in an atmosphere terminated at 220 km by a free surface is

$$\langle p_0 \rangle = \int_0^\infty \delta w_s \frac{N_A^{(1)}}{F_A} N_A^{(2)} dk, \tag{1}$$

where

$$\left.\begin{aligned} N_A^{(1)} &= -A_{21}, \\ F_A &= A_{22}, \\ \delta w_s &= \frac{L(\omega)}{2\pi} J_0(kr).k\, e^{i\omega t}, \end{aligned}\right\} \tag{2}$$

ω is the angular frequency and k is the angular wave number. The subscripted elements of the n layer product matrix A and $N_A^{(2)}$ are the same as in Harkrider (1964). The transformed source-time function is $L(\omega)$ and will be discussed later.

The far-field solution of excess pressure is given by the residue contribution of (1). Thus we obtain for each mode or k_j root, ω fixed, of $A_{22}=0$

$$\{p_0\}_j = i \frac{L(\omega)}{2} .k_j \left[\frac{p(H)}{p_0}\right] G(\omega).H_0^{(2)}(k_j r)\, e^{i\omega t}, \tag{3}$$

where

$$G(\omega) \equiv \frac{A_{21}}{(\partial A_{22}/\partial k)_{\omega,j}}$$

and $p(H)/p_0$ is the excess pressure ratio of the far field at source height H relative to that at the rigid surface.

The velocity and pressure ratios are related to the computed layer product matrix $A(z)$ by

$$\left[\frac{w^*(z)}{p_0}\right] = [A(z)]^*_{12},$$

$$\left[\frac{p_\rho(z)}{p_0}\right] = [A(z)]_{22},$$

and

$$\left[\frac{p(z)}{p_0}\right] = [A(z)]_{22} + \frac{\rho^0(z) g}{\omega} [A(z)]^*_{12}.$$

The n layer product matrix A is given as

$$A = A(220).$$

A more detailed description of the layer matrices and their properties can be found in Press & Harkrider (1962) and Harkrider (1964).

In the limit as the source location approaches the Earth's surface, this source reduces to that of Pekeris (1939). The Pekeris model is the rigid surface vertical velocity source

$$w_{so}(0)=\frac{L(\omega)}{2\pi}\,e^{i\omega t}\int_0^\infty J_0(kr)\,k\,dk, \tag{5}$$

which is zero everywhere on the horizontal plane except at the origin.

The linearized equations governing the vertical dependence of the excess pressure p in a constant velocity (α) gravitating liquid such as the ocean can be written as

$$\frac{d^2p}{dz^2}+\frac{g}{\alpha^2}\frac{dp}{dz}+\left(\frac{\omega^2}{\alpha^2}-hk^2\right)p=0, \tag{6}$$

where $h=1-(\sigma_2/\omega)^2$, g is the gravity field strength, and σ_2 is the Brunt frequency.

The vertical particle velocity for such a medium is related to p by

$$\frac{dp}{dz}+\frac{g}{\alpha^2}p=-i\omega h\rho^0 w, \tag{7}$$

where ρ^0 is the ambient density.

Comparing (6) and (7) with their respective relations for an isothermal gravitating atmosphere (Harkrider 1964), we see that the atmospheric equations reduce to (6) and (7) if we let the specific heat ratio γ approach unity in all relations except in the definition of the Brunt frequency.

Therefore, by setting $\gamma=1$ except in the Brunt frequency we are able to include a gravitating liquid as part of the atmospheric layering. This allows us to extend the acoustic–gravity theory and the numerical matrix techniques of calculating dispersion and source excitation to a system in which the ocean is the lower part of the layered wave guide.

With the rigid surface $z=0$ now at the ocean bottom, we place the source and receiver at sea level $z=H$ and the excess pressure there is given from Harkrider (1964) as

$$\{p(H)\}_j=i\frac{L(\omega)}{2}k_j\left[\frac{p(H)}{p_0}\right]^2 G(\omega)H_0^{(2)}(k_jr)\,e^{i\omega t}, \tag{8}$$

with a sea displacement of

$$\{q(H)\}_j=D(\omega).R(\omega)\{p(H)\}, \tag{9}$$

where the 'dynamic ratio' $D(\omega)$ is

$$D(\omega)\equiv\frac{1}{\omega}\left[\frac{w^*(H)}{p_0}\right]\Big/\left[\frac{p_\rho(H)}{p_0}\right], \tag{10}$$

and the ratio of Lagrangian pressure to Eulerian pressure at $z=H$ is

$$R(\omega)=\left[\frac{p_\rho(H)}{p_0}\right]\Big/\left[\frac{p(H)}{p_0}\right]. \tag{11}$$

The spectra and time series were calculated for two Fourier-transformed source functions. The first time function was a delta function which corresponds to

$$L(\omega)=1. \tag{12}$$

The second was a single cycle of a sine wave

$$f(t)=\begin{cases} 0 & t<0 \\ \sin(2\pi t/T) & 0\leqslant t\leqslant T \\ 0 & t>T, \end{cases} \tag{13}$$

which yields

$$L(\omega)=\int_{-\infty}^{\infty} f(t)e^{-i\omega t}dt$$

$$=\frac{4\pi}{T}e^{-i(\omega T/2+\pi/2)}\sin(\omega T/2)/(\omega^2-4\pi^2/T^2). \tag{14}$$

Correcting for curvature and integrating over ω so that the source has the desired velocity variation in time, we obtain at large distances from the source

$$[p(\theta, H;\ t)]_j=\frac{1}{2\pi}\int_{-\infty}^{\infty} L(\omega)I_j(\omega)\,e^{i(\omega t-k_j r+3\pi/4)}d\omega \tag{15}$$

and

$$[q(\theta, H;\ t)]_j=\frac{1}{2\pi}\int_{-\infty}^{\infty} L(\omega).D_j(\omega).R_j(\omega)I(\omega)\,e^{i(\omega t-k_j r+3\pi/4)}d\omega, \tag{16}$$

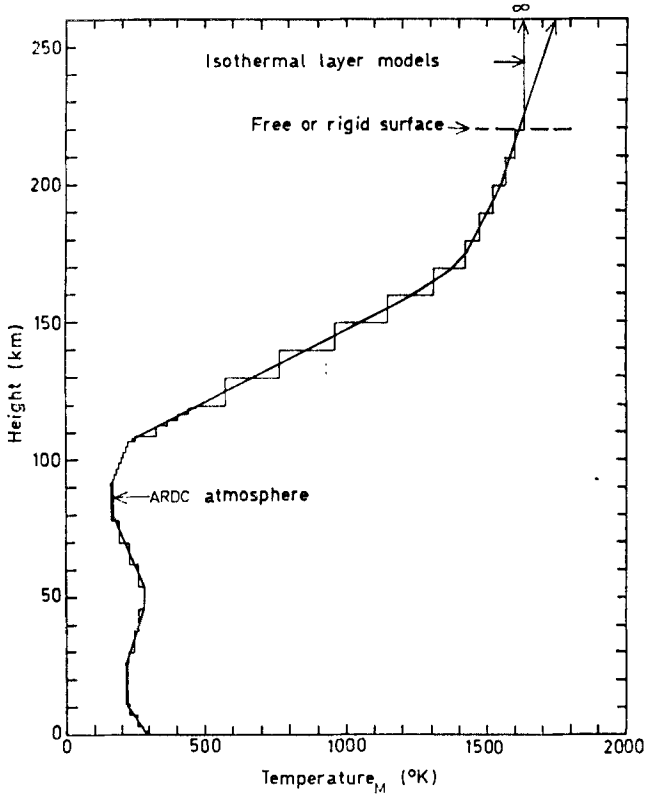

FIG. 1. ARDC standard atmosphere to which ocean was added for calculations. Also shown is its approximation by isothermal layers.

where

$$I_j(\omega) = \left(\frac{k_j}{2\pi a_e \sin\theta}\right)^{\frac{1}{2}} \left[\frac{p(H)}{p_0}\right]^2 G_j(\omega), \tag{17}$$

θ is the colatitude, a_e is the Earth's radius, and r is now the distance from the source measured on the surface of the Earth; i.e. $r = a_e.\theta$.

The theoretical barograms and marograms given by (15) and (16) are calculated by means of two Fortran programs written for the IBM 360/50H computer. These programs are the same as those described in detail in Press & Harkrider (1962), and Harkrider (1964) with two exceptions. (1) The input parameters for the ocean are layer thickness, acoustic velocity, density and Brunt frequency instead of the layer thickness and temperature used for the description of the layered atmosphere. (2) The program sets $\gamma = 1$ and uses the input Brunt frequency in all matrix element calculations involving ocean layers.

3. Numerical results

The model used in the calculations consists of a standard ARDC atmosphere underlain by a constant-density, constant-velocity ocean. The atmosphere was terminated with a free surface and the ocean bottom was assumed to be perfectly rigid (Fig. 1). The explosive source was placed at the surface and its time variation was taken as a delta function or as a single cycle of a sine wave with period ranging from 10 to 120 minutes. Although this is somewhat arbitrary, the observed barometric pulse shapes are suggestive of such a source.

The phase velocity (dashed) and group velocity (solid) curves for the atmosphere alone and the ocean alone are shown in Figs. 2 and 3 respectively. The atmospheric curves show the acoustic (S) modes and the gravity (GR) modes. The S modes exist even when gravity is reduced to zero, whereas the GR waves vanish for this case. An interesting feature is that the flat segments of phase and group velocities of S_1, S_0 and GR_0 are nearly connected to form a common group velocity curve, which accounts for the main feature of the Krakatoa air wave—its velocity and its pulse-like character.

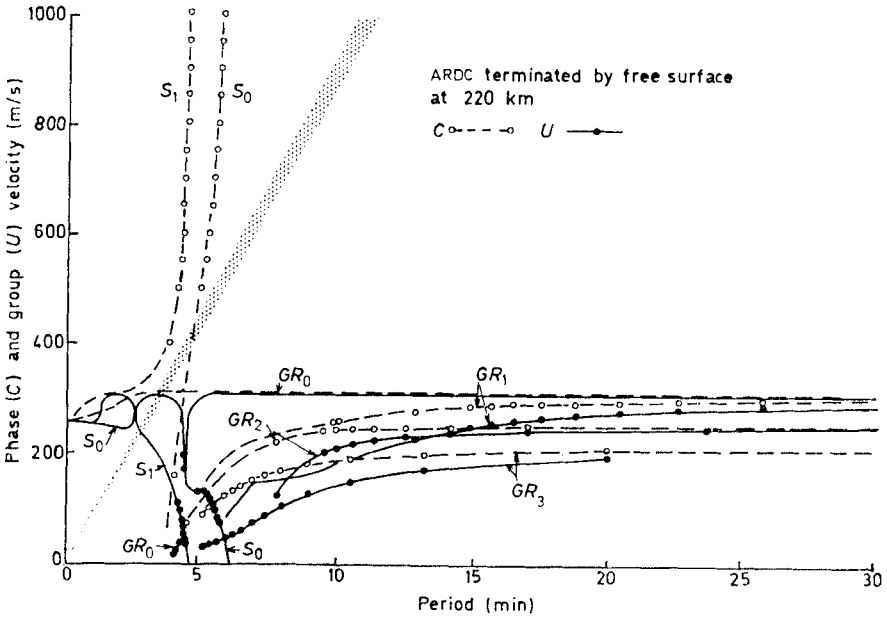

FIG. 2. Phase and group velocity dispersion curves for several modes of ARDC standard atmosphere with free surface at 220 km.

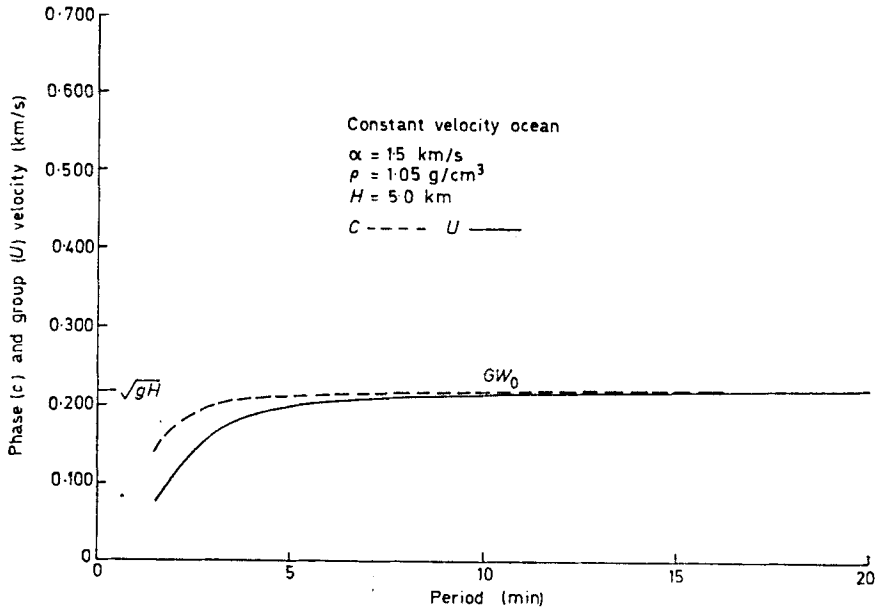

FIG. 3. Phase and group velocity dispersion curves for fundamental gravity wave in a constant-velocity, constant-density ocean of 5 km thickness.

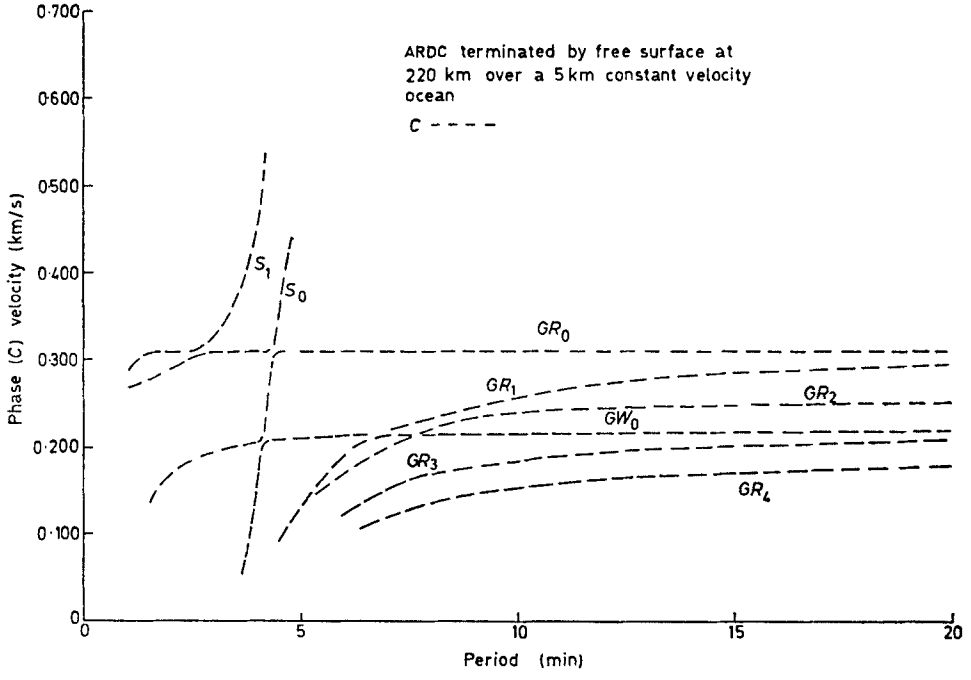

FIG. 4. Phase velocity dispersion curves for modes of the air–ocean system.

Only the classical gravity surface waves are shown for the ocean in Fig. 3, the long wave phase and group velocity being given by the $\sqrt{(gH)}$. Several interesting features emerge when the two systems are coupled as shown in Figs. 4 and 5. The characteristics of the individual systems are retained in pseudo-dispersion curves consisting of segments of the continuous modal curves of the coupled system. Thus, the GW_0 mode of the separate ocean system is duplicated by joining segments of GW_0, GR_2, GR_1 and GR_0 of the coupled system.

These dispersion curves lead us to expect a continuous sequence of arrivals, beginning with the atmospheric pulse (312 m/s), continuing to the ocean gravity wave (220 m/s) and persisting for a long time thereafter. Without a discussion of excitation functions we are unable to specify the distribution of energy in the ocean and atmosphere for the different modes.

A quantity called the dynamic ratio may be defined which is the ratio of displacement to pressure at the air–ocean interface. This ratio has the approximate value of 1 for the hydrostatic case and is therefore a convenient measure of dynamic coupling as a function of phase velocity, period or arrival time. Dynamic ratio curves are shown in Fig. 6, the numerical values being indicated also by numbers located on the dispersion curves of Fig. 5 at the periods for which they were calculated. The principal effect seen is the large dynamic ratios found where the phase velocity is near $\sqrt{(gH)}$. Dynamic ratios at least ten times greater than hydrostatic are found in the phase velocity range 195–230 m/s. When plotted as a function of group delay, dynamic ratio values imply an increasing transfer of energy from the atmosphere to the ocean following the arrival of the initial air pulse. For a station as far as San Francisco (Fig. 6, right side), waves with dynamic ratios greater than 10 begin to arrive about 6 hours after the initial air pulse.

Dynamic ratios and dispersion indicate displacement–pressure values at the air–sea interface, and phase and group characteristics of all possible modes. It remains to

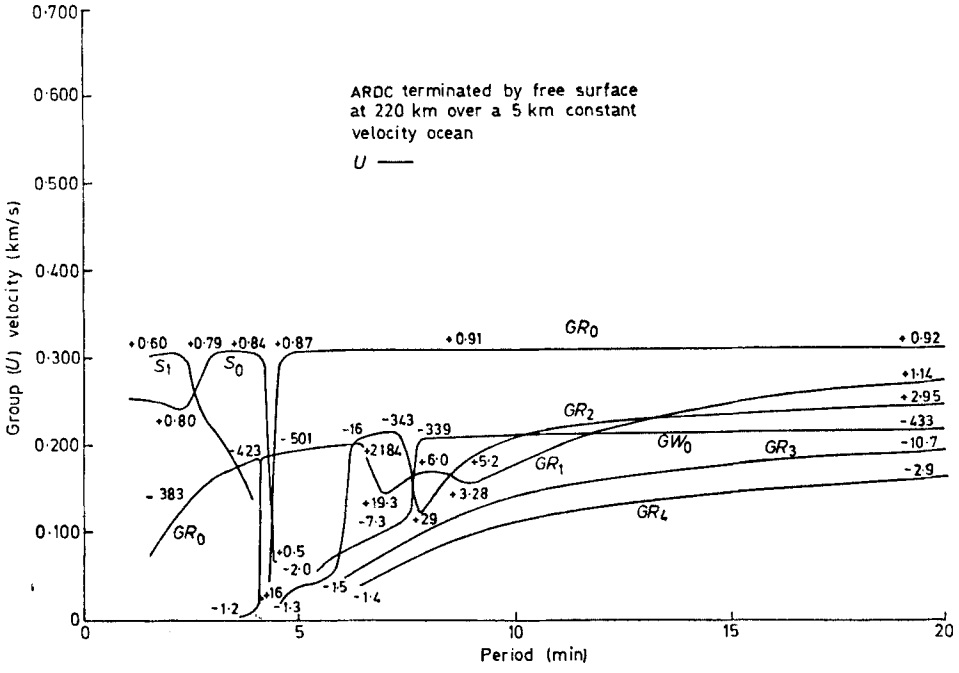

FIG. 5. Group velocity dispersion curves for several modes of the air–ocean system. The numbers shown are the dynamic ratios at their corresponding periods.

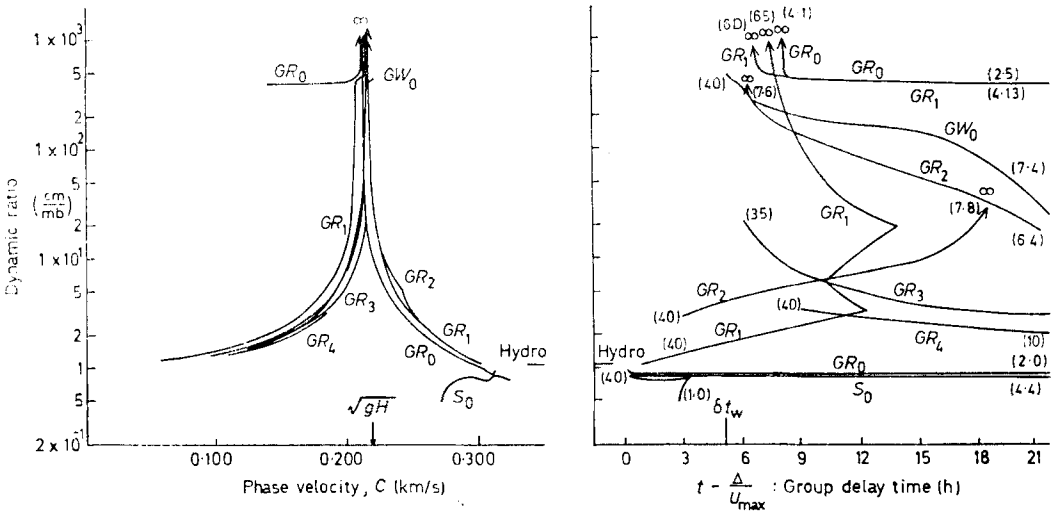

FIG. 6. Dynamic ratio as a function of phase velocity (left) and group delay with respect to first arrival at San Francisco (right). U_{max} is equal to 312 m/s and Δ is 14 053 km. The numbers in parentheses indicate the period ranges of the curves.

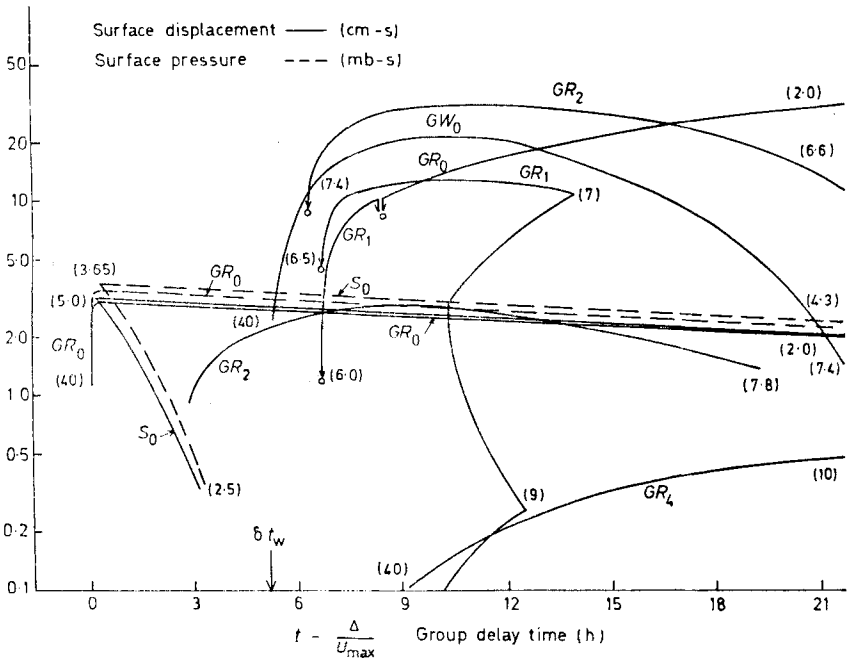

FIG. 7. Spectra of sea level displacements and air pressures for several modes excited by a surface explosion with a delta function time variation. Abscissa is group delay with respect to first arrival in San Francisco.

discuss which portions of the different modes are excited by a specific source. The relative excitations of several modes are shown in Fig. 7 for the case of a surface source with a delta function time variation. The abscissa is time following the first arrival for a station distance of 14053 km (San Francisco). It is seen that the first arrival is an atmospheric pulse and a sea wave with dynamic ratio close to the hydrostatic value of 1. Contributions from GR_0 and S_0 make up this signal. The oscillations continue at about the same level until the time $\delta t_w = \Delta/\sqrt{(gH)} - \Delta/U_{max}$ (where Δ is the distance and U_{max} is 312 m/s) when the water waves increase several-fold in amplitude. The numbers in parentheses indicate periods of the waves at the times indicated.

Finally, a synthetic barogram and a synthetic marigram are shown in Fig. 8 for a surface source with time variation of a single-cycle sine wave of period 40 minutes. Instrumental response was assumed to be flat and the distance corresponds to that of San Francisco. The main effects, already discussed, appear in the records. The initial pulse is a transient and shows as a disturbance in the atmosphere and ocean. This is the main Krakatoa pulse which was observed at many places over the world. It is formed almost entirely from the GR_0 mode. The second event also shows on the barogram and marigram and is a contribution from the mode GR_2. Finally, the largest disturbance of sea level occurs with the arrival of the GW_0 mode with hardly any pressure pulse accompanying it. However, the sea wave is excited by atmospheric waves with the same phase velocity, although they are not apparent on the record because of the large dynamic ratio. We have computed synthetic records for other source-time functions. The character changes as would be expected because different segments of modes are excited. However, the largest sea waves always correspond to the GW_0 mode.

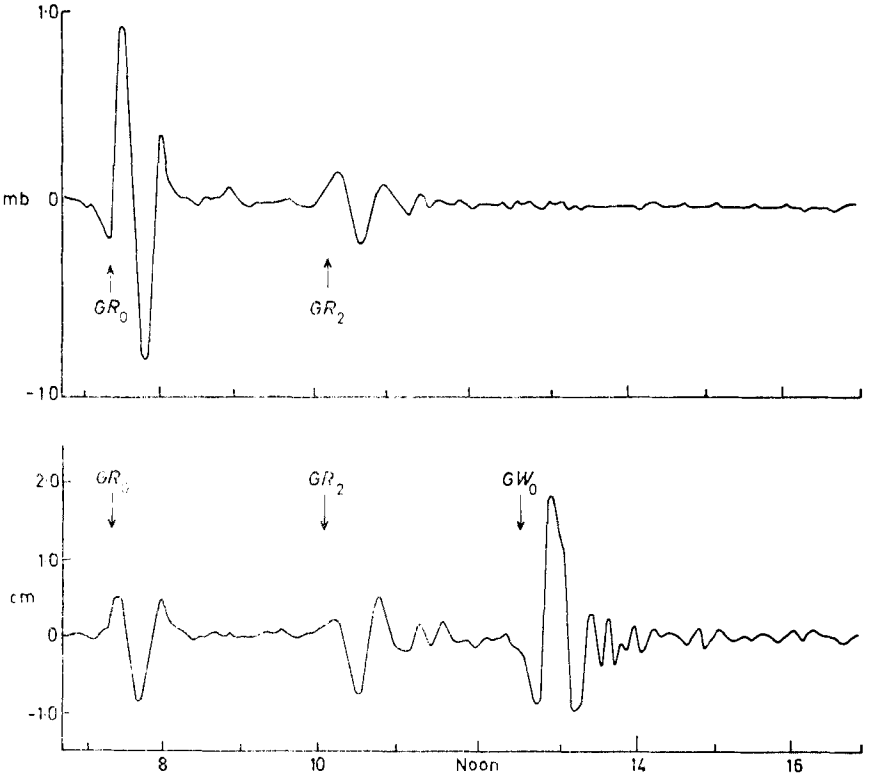

FIG. 8. Synthetic barogram (upper) and marigram (lower) for San Francisco. Source time function is a single-cycle sine wave of 40 minute period. Time is local time, 1883 August 27.

4. Discussion

The responses of the barographs and tide gauges which recorded the Krakatoa signals in 1883 are not known to us. There is reason to believe that non-linear responses may be involved, because the instruments were driven at higher frequencies than anticipated in their design. Furthermore, the tide gauges may have been responding to resonances in the harbour excited by the sea waves. For these reasons we can only make a qualitative comparison of the theory with the observations.

A selection of marigrams is shown in Fig. 9, redrawn from Symons (1888). The arrows indicate the theoretical arrival times of the modes GR_0 and GW_0. Also indicated at the theoretical arrival times of tsunami which follow least-time paths around obstacles formed by continents, archipelagos, etc. As pointed out by others (see, for example, Ewing & Press 1955), except for South Georgia, the tide gauge disturbance occurred much too early to be explained as tsunami, the discrepancy being of the order of 10 hours. Moreover, the paths to Colon, Honolulu, San Francisco and the English Channel ports require such circuitous routes and passage across barriers as to eliminate the possibility of tsunami action. Excitation by the atmospheric pulses is almost a necessity.

It seems reasonable to conclude that the main Krakatoa atmospheric pulse corresponds to propagation in the GR_0 mode of the atmosphere. The corresponding sea

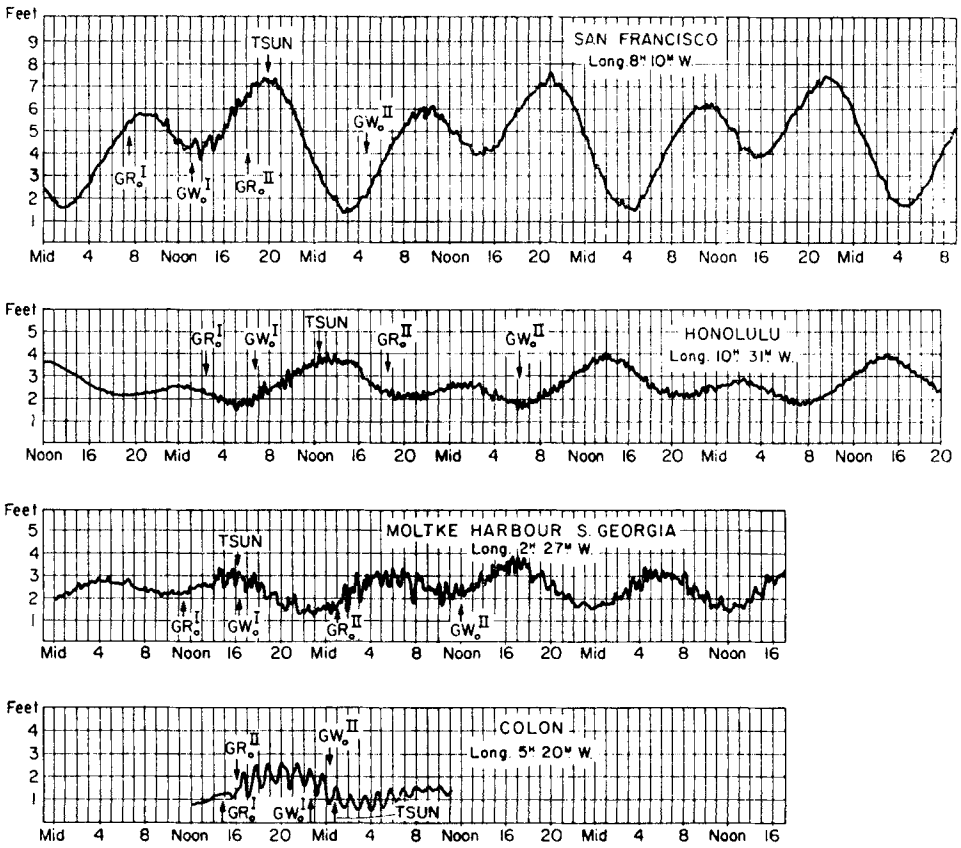

FIG. 9. Marigrams for San Francisco, Honolulu, South Georgia and Colon. Arrows indicate theoretical arrival times of several modes and the tsunami. Roman superscripts indicate short (I) and long (II) great circle paths. The ordinate is feet. Abscissa is local civil time beginning 1883 August 27 except Honolulu, which begins August 26.

disturbance is essentially hydrostatic. The main sea waves are in the GW_0 mode and propagate along great circle paths with phase velocities near $\sqrt{(gH)}$. These are excited by atmospheric waves with the phase velocities near $\sqrt{(gH)}$. Intervening land barriers are 'jumped' by the air waves, which can re-excite the sea wave if a sufficiently long fetch is available.

Using the scaling methods of Harkrider (1964) and data from nuclear explosions, we estimate that a surface explosion amounting to about 100–150 megatons would produce pressure pulses equivalent to those observed from Krakatoa.

Acknowledgments

This research was supported by the Advanced Research Projects Agency and was monitored by the Air Force Office of Scientific Research under contracts AF 49(638)–1632 with the Massachusetts Institute of Technology and AF 49(638)–1693 with Brown University.

Department of Geological Science,
Brown University,
Providence,
Rhode Island,
U.S.A.

Department of Geology and Geophysics,
Massachusetts Institute of Technology,
Cambridge,
Massachusetts,
U.S.A.

References

Ewing, M. & Press, F., 1955. *Trans. Am. geophys. Un.*, **36,** 53.
Harkrider, D. G., 1964. *J. geophys. Res.*, **69,** 5295.
Pekeris, C. L., 1939. *Proc. R. Soc.*, A, **171,** 434.
Press, F. & Harkrider, D. G., 1962. *J. geophys. Res.*, **67,** 3889.
Symons, G. (ed.), 1888. *The Eruption of Krakatoa and Subsequent Phenomena.* Trubner, London.